Journal of Structural Geology, Vol. 12, No. 3, pp. 303 to 314, 1990
Printed in Great Britain

0191-8141/90 $03.00+0.00
Pergamon Press plc

Extensional reactivation of an abandoned thrust: a bound on shallowing in the brittle regime

E. R. IVINS, T. H. DIXON and M. P. GOLOMBEK

Earth and Space Sciences Division, Jet Propulsion Laboratory, California Institute of Technology, Pasadena, CA 91109, U.S.A.

(*Received* 10 *June* 1988; *accepted in revised form* 2 *October* 1989)

Abstract—Shallow dip angles (≤45°) suggested by field observations of continental extensional faults are not predicted by classical isotropic Mohr–Coulomb–Anderson theory. Earthquake data indicate that normal faults exist in the upper crust with dip angles commonly as shallow as 30°. Some structural evidence suggests brittle-normal faulting with dip angles as shallow as 10°. One explanation of the apparent conflict between theory and structural/seismic observations is that intrinsically weak, shallow-dipping pre-existing faults are preferentially reactivated. Any reduction in frictional strength of the pre-existing structure below that of surrounding rock increases the likelihood that such structures will be first breaking when extension is initiated. Enhanced fluid pore pressure on the pre-existing fault reduces the effective strength and can further enhance shallow fault reactivation. An analytical treatment clarifies the roles of geometry, intact/pre-existing fault strengths and fluid pore pressures. Frictional strength ratios of 3 or greater could account for extremely shallow normal faults (dips 10–20°) *without* consideration of pore pressures in excess of the least principal stress *or* of principal stress systems rotated away from the gravity vector. Moderate reduction in friction ($\frac{3}{4}$) with respect to wall rock can reduce the dip to 30° and can account for shallow normal-slip earthquakes.

INTRODUCTION

THE origins of major tectonic structures and the occurrence of intraplate earthquakes may be strongly influenced by pre-existing weak zones (McKenzie 1969, Sykes 1978, Bergman & Solomon 1980, Dixon *et al.* 1987). Reactivation of extinct thrust structures is often cited as the nucleation source for normal and/or oblique-slip faulting occurring at angles that significantly deviate from those predicted by classical Mohr–Coulomb–Anderson theory (Doser 1987). Normal faults in intact rock are predicted to be steeply-dipping (≈60°). The basal faults associated with thrusting in a compressional regime are predicted to be of relatively shallow dip (≤25°); a fact generally born out by numerous structural and seismic observations (Davis *et al.* 1983, Suppe 1985, p. 280, Webb & Kanamori 1985). It has been suggested that the shallow dips of many normal faults in an extensional tectonic environment are due to the reactivation of intrinsically weak (and geometrically viable) pre-existing thrusts or other planes of weakness (Sykes 1978, Brewer & Smythe 1984, Smith & Bruhn 1984, Allmendinger *et al.* 1987, Doser 1987, Enfield & Coward 1987).

The idea that a low-angle weak zone may be brittlely reactivated in a newly initiated extensional stress environment motivates the analysis presented in this paper. The theoretical method parallels that of Zoback & Zoback (1980) who studied reactivation of pre-existing faults in the central Basin and Range province where the regional principal stress was relatively well-constrained. Their analysis demonstrated that reactivation of pre-existing structures was intimately tied to the frictional strength reduction on the misaligned surface and to the ambient fluid pore pressure. In the study presented below we retain the general geometrical representation of the fourth-rank rotational tensor operation on the second-rank background, or tectonic, stress tensor field. Additionally, the analysis retains finite contrasts in cohesive strength between intact and previously faulted rock. Contrasts between fluid pore pressures at the fault surface and the surrounding intact rock are also accounted for. Any enhanced pore pressure existing on the previously faulted surface may provide the extra effective frictional strength reduction necessary to reactivate low-angle structures. These three new features of the analysis (geometry, contrasting brittle strength parameters and enhanced pore pressure) allow us to examine a very fundamental question: how shallow, and under what conditions may an abandoned thrust fault be brittlely reactivated in an extensional tectonic environment? What is derived in this paper constitutes a first-order analysis, incorporating only the simplest assumptions concerning tectonic stress and empirically derived failure criteria.

STABILITY AND STRENGTH OF A SHALLOW-LYING FAULT

Seismic and structural evidence

Mohr–Coulomb–Anderson theory predicts that initial normal faults form with dip, $\Delta = \pi/4 + \tan^{-1}(\mu)/2$. For unfractured rock μ is the coefficient of internal friction and is related to the empirically derived angle of internal friction, Φ, with $\mu = \tan\Phi$. For a crust filled with randomly oriented pre-existing fractures and joints, this dip angle, Δ, is that most susceptible to initial normal

faulting and μ is the coefficient of static (or sliding) friction (e.g. Price 1966). Coefficients of internal (Coulomb) friction typically vary from 0.36 to 1.0 and predict normal fault dip to be in the range 55–68°. If brittle strength is characterized by the static friction of pre-fractured rock (Byerlee's Law) then the dip predicted by isotropic Mohr–Coulomb–Anderson (henceforth, 'MCA') stability theory is about 60–65°. Indeed, many continental earthquakes in zones of active extension originate at surfaces of steep dip, including the most recent and well-documented large event of this type: the Borah Peak earthquake in the northern Basin and Range province (Barrientos *et al.* 1987). Most well-recorded normal faulting earthquakes originate on surfaces with dips in the 30–60° range (Jackson 1987a,b). Using data from 28 well-recorded earthquakes in the Basin and Range, Arabasz & Julander (1986) determined that both mean and median dip angles of normal-slip events are in the range 49–59°. The data reported by Arabasz & Julander (1986) are consistent with MCA theory, considering the statistical variability produced by all pre-existing weaknesses (McKenzie 1969, Donath & Cranwell 1981, Rundle 1988). However, normal-slip events occurring with dip angles near 30° are in substantial disaccord with the prediction of MCA theory (55–68°).

Many structural field studies cite pre-existing planes of weakness as having significant control on subsequent faulting (e.g. Price 1967). Some examples are thrust faults reactivated as normal faults. Ratcliffe *et al.* (1986) find structural evidence within the Musconetcong thrust system of Pennsylvania for early Mesozoic extension on a Paleozoic low-angle thrust fault. Coward (1988) found evidence that the deformation history of the Outer Hebrides fault in the Scottish Caledonides includes a phase in which a shallow thrust is reactivated as a normal fault. Counterexamples, where shallow thrusts are cut by new and extremely low-angle normal faults, have been found in two recent field studies: Wernicke *et al.* (1985) shows that young, 20–25° dipping normal faults cut across older thrust structures in the Mormon Mountains of southern Nevada, and Burchfiel *et al.* (1983) discovered a similar cross-cutting relation in the Kingston Range in California. Below anisotropic MCA theory is used to try to quantify how weaker pre-existing faults may become reactivated. Such a theory will only explain some subset of shallow normal faulting because, clearly the basic premise is at odds with observations such as those described by Wernicke *et al.* (1985). However, the derived relations establish some criteria under which reactivation *will* and *will not* occur, thereby providing constraints on one attractive explanation of low-angle normal faulting.

Anisotropic MCA theory

The anomalous conditions that may lead to the brittle reactivation of an extremely shallow normal fault have been examined by Bruhn *et al.* (1982) and Sibson (1985). Their analyses indicated that shallow dips (≤35°) are possible only if very low coefficients of static friction exist (<½ of the values typical of Byerlee's Law). They also emphasized the role that tensile failure can play if pore pressure, P, exceeds σ_3, the least principal stress. In this paper we focus attention to the case of shear failure and present an analysis that generalizes the studies of Bruhn *et al.* (1982) and Sibson (1985). The susceptibility to shallow reactivation is more clearly quantified when additional contrasts between intact and previously faulted rock are retained in the analysis.

Etheridge (1986) has noted that rock within exhumed ductile shear zones may be characterized by substantially reduced brittle frictional strength in the direction parallel to foliation. Hydrothermal alteration often characterizes cataclasites (crustal rocks associated with intense brittle phenomena) and anomalously large pore pressures may have existed at the time of formation (Sibson 1981, Parry & Bruhn 1986). Active low-angle thrusts may localize extreme concentrations of water (Heard & Rubey 1966, Cloos 1984, Vrolijk 1987). For these reasons we incorporate into the analysis the potential for finite contrast between intact wall rock pore pressure, P, and fault rock pressure, $P + \delta P$, where δP is the excess pressure existing within the fault zone. A description of how faults might actually maintain an excess pressure δP is complex (e.g. Price 1977, Raleigh & Marone 1986) and is beyond the scope of the present paper.

The parameters characterizing the pre-existing fault

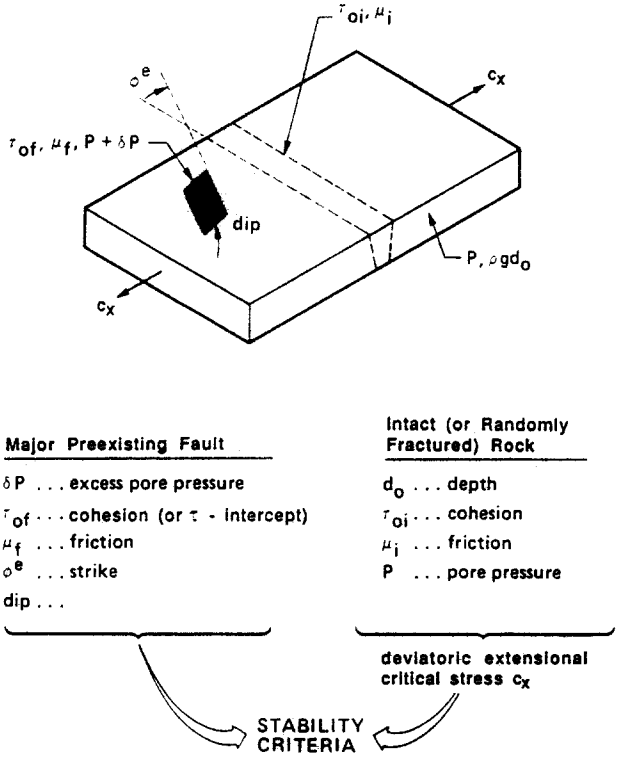

Fig. 1. Geometry and strength parameters. Crustal segment is under extensional forces, c_x, acting at a distance. The pair of dashed lines represent predicted attitudes of either newly breaking ('Anderson') normal faults or of optimally oriented pre-existing fractures of strength characterized by Byerlee's Law. (See Fig. A1 of Appendix A for coordinate frame definitions.) The shaded plane shows the orientation of a major pre-existing fault or other plane of weakness.

stability state are shown in Fig. 1. A single low-angle structure is potentially destabilized (reactivated) by extensional deviatoric tectonic forces acting at a distance. The friction, μ, and cohesion, τ_o, are subscripted 'i' and 'f' for intact and faulted rock, respectively. We assume that 'intact' rock is defined either by unfractured rock (i.e. the Coulomb–Mohr envelope, e.g. Engelder & Marshak 1988, p. 209) *or* by a pervasively fractured crust with failure envelope given roughly by Byerlee's Law. Prefractured rock may often be viewed as relatively 'intact' when contrasted to rocks like gouge that characterize major faults. Cohesional and frictional strength variation are best represented by the ratios τ_{of}/τ_i, and μ_f/μ_i, respectively. Strictly speaking, the values μ_i, τ_{oi} and μ_f, τ_{of} rely on linear fits to laboratory data. Finite τ_o in Byerlee's Law, for example, is simply the τ-intercept and does not represent a true cohesion. However, it seems reasonable to suspect some degree of cohesive annealing on pre-existing faults (Zoback & Zoback 1980).

By convention, the pre-existing fault strike is misoriented from that of potential steep-angle normal faults (dashed in Fig. 1) by an angle, ϕ^e. The tectonic stress, c_x, acting in the opposite direction to the total minimum principal stress, σ_3, will initiate the steep-angle normal faults (dashed) in the absence of precipitous motion on the pre-existing zone of weakness. Further assumptions about the stress system are discussed in Appendix A and in the section below.

Mohr diagram

A competition between potential new faults and misoriented pre-existing structures forms the stability analysis. As demonstrated in Appendix B, when the pre-existing fault possesses the same strike as that of the potential new normal faults ($\phi^e = 0°$) then the stability problem can be defined in terms of the two-dimensional Mohr diagram shown in Fig. 2(a). Aside from misalignment in trend (finite ϕ^e), all of the essential ingredients of the analysis are described in Fig. 2(a). Here τ is the shear stress and $\sigma - P$ is the effective normal stress resolved on the fault surface. The reference state of the stability analysis is that characterizing the onset of new faulting in intact rock. This state is defined in the Mohr diagram by the line tangent to the circle at the position indicated by the label '*' in Fig. 2(a). Here the stability analysis deviates from that of Bruhn *et al.* (1982) and Sibson (1985). By defining the reference state in this way, the positions, $\sigma_1 - P$ and $\sigma_3 - P$, are uniquely specified by four quantities: the common depth of initiation, d_o (defining σ_1, see Appendix A); the cohesion of intact rock, τ_{oi}; the friction of intact rock, μ_i; and the pore pressure, P, that exists in the intact rock. We nondimensionalize all quantities having units of stress (MPa) by the scale factor $(1/\sigma_1)$. Any term rescaled in this way is superscripted with a prime ('). The analysis parallels that of Jaeger (1960) who discussed MCA stability theory for rock containing anisotropic planes of weakness.

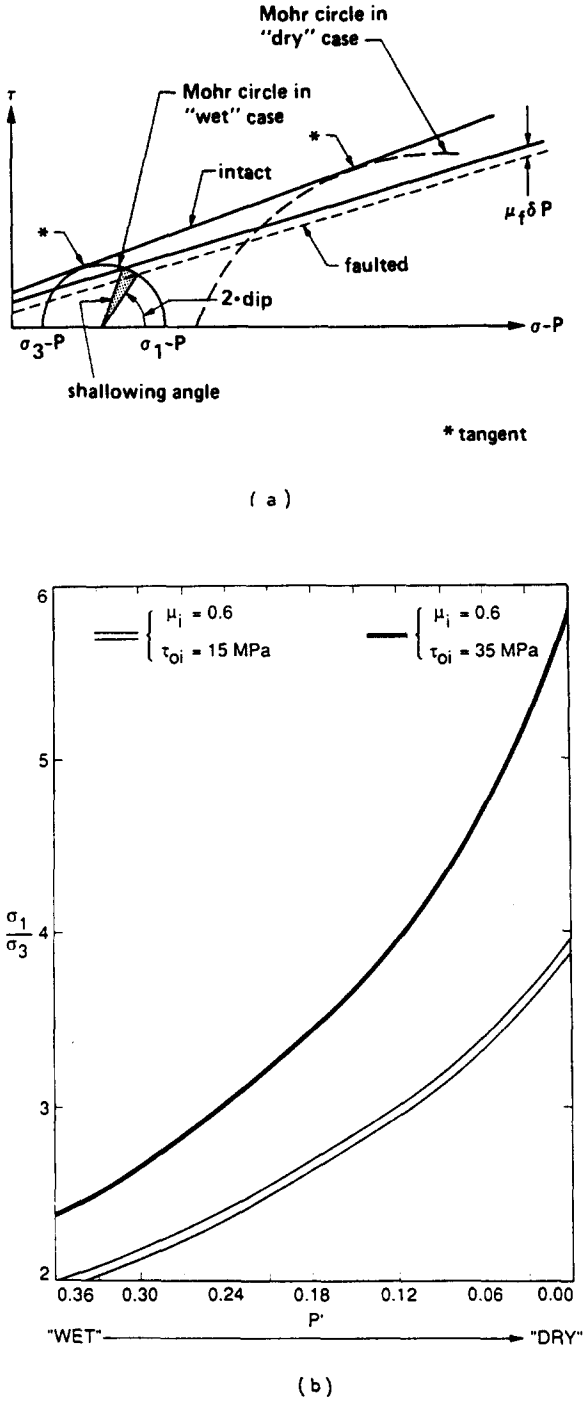

Fig. 2. Mohr circle for anisotropic MCA stability analysis (a) and stress states, $\sigma_1/\sigma_3(S_r^{-1})$, as a function of intact rock dimensionless fluid pore pressure (b) where $P' \equiv P/\sigma_1$. For dry intact rock ($P' \to 0$) the sustainable mean stress, $(\sigma_1 + \sigma_3)/2$, of intact rock increases, thus increasing the likelihood that enhanced fluid pressure on the fault surface, δP, will have an important role in destabilizing the pre-existing fault. See Fig. 1 for other rock parameter definitions and text for interpretation of the three lines and shaded shallowing angle shown in (a). As discussed in the text, 'intact' rock may be governed by either a Coulomb–Mohr envelope or by a failure envelope for rock obeying Byerlee's Law.

It is the contrast in rock properties that can now be assessed, as the magnitude of the tectonic-driving force is simply a function of the ratio of minimum to maximum principal stresses, S_r (see equations A2, A5 and B2 of Appendices A and B, respectively). The two lines drawn below that for intact rock shown in Fig. 2(a) represent

the failure envelope for faulted rock of decreased friction and cohesion (solid) and for faulted rock that additionally is weakened by an enhanced pore pressure, δP, in excess of that in the surrounding rock (dashed). The amount of strength reduction caused by excess pressure, δP, can be measured as a change in height of the envelope by an amount, $-\mu_f \delta P$ (see Fig. 2a, upper right, and the τ-axis intercept in Fig. B1). This general approach to excess pore pressure has been discussed by Hill (1982). In this regard, it is important to point out that it is the space τ vs $\sigma - P$ where stability must be tested. For this reason we do not 'slide' the Mohr circle to the left as in the classic treatment of pore pressure effects (cf. Secor 1965).

The angle measured from the $\sigma - P$ axis counterclockwise along the Mohr circle for intact rock to the point of tangency (*) is twice the dip angle of a potential new 'Anderson' fault or of a pre-existing fracture of optimum orientation for reactivation. Dip angles that are possible due to a weaker competing fault are delineated by the arc that sweeps past the tangent point (*) and connects the two intersection points of the 'weak' failure envelope with the Mohr circle. Half the counterclockwise angle to the first of these intersection points defines the *shallowest possible dip*. Any additional decreased strength then implies further dip reduction. An example of additional shallowing due to enhanced pore pressure is shown by the shaded portion of the Mohr circle in Fig. 2(a). Two curves plotted in Fig. 2(b) show a range of $\sigma_1/\sigma_3(1/S_r)$ using varying dimensionless intact pore pressure, $P' \equiv P/\sigma_1$, for 'intact' rock parameters typical of Byerlee's Law. This variation between 'wet' and 'dry' extremes will define part of the parameter space relevant to the investigation.

The two-dimensional Mohr diagram (Fig. 2a) facilitates a description of the MCA stability analysis applied to anisotropic pre-existing planes of weaknesses. This two-dimensional analysis has been reviewed by Donath & Cranwell (1981) and has been applied to laboratory studies by Handin (1969). The two-dimensional analysis can be generalized to three dimensions. Critical to determining this useful generality is giving precise definition to the marginal stability state. This is described in detail in Appendix B and is introduced below.

THREE-DIMENSIONAL THEORY: A LOWER BOUND

The shallowest possible dip, δ, of a pre-existing, anomalously weak, fault that is in equal competition with the breakage of new faults will be given by the marginal stability state. This state is defined by equating the resolved shear on the pre-existing fault to the critical value of the shear stress needed to initiate failure. This state is discussed at length in Appendix B with the concluding equation (B7) representing the mathematical statement of this condition. A key element of this statement is the recognition that the stress ratio, S_r, is a function of intact rock parameters (see equation B2). On the pre-existing weaknesses the condition is:

$$\mu_f \sin^2\delta(S_r \cos^2\phi^e + \sin^2\phi^e) + \mu_f \cos^2\delta + \tau'_{of} - \mu_f(P' + \delta P') + (S_r \cos^2\phi^e + \sin^2\phi^e - 1)\cdot \cos\delta \sin\delta = 0. \quad (1)$$

Obtaining the minimum allowed dip, δ, is then reduced to finding a solution to the transcendental equation (1). This is a trivial procedure provided one uses a rotational transformation through an angle, θ, that eliminates the cross term, $\cos\delta \sin\delta$, from equation (1). The angle of this rotation is:

$$\theta = -\frac{\pi}{4} + \frac{1}{2}\tan^{-1}(\mu_f) \quad (2)$$

and applying this transformation the transcendental equation is reduced to

$$(1 + \mu_f^2)^{1/2}\cos^2(\delta - \theta) = -\mu_f(1 - S_r)^{-1}[\tau'_{of}/\mu_f - (P' + \delta P' - 1)]/\cos^2\phi^e + \mu_f \cos^2\theta - \tfrac{1}{2}\sin 2\theta.$$

Further reduction is accomplished by using the expression for S_r in terms of intact parameters (equation B2). The reduction yields

$$\cos 2(\delta - \theta) = (1 + \mu_f^2)^{-1/2}\cdot\{\mu_f - [\mu_i + (1 + \mu_i^2)^{1/2}]\cdot[(\mu_f/\mu_i)(P' + \delta P' - 1 - \tau'_{of}/\mu_f)/(P' - 1 - \tau'_{oi}/\mu_i)]/\cos^2\phi^e\}. \quad (3)$$

An important ratio is revealed in equation (3) that isolates all pore pressure effects:

$$H = (1 - P' - \delta P' + \tau'_{of}/\mu_f)/(1 - P' + \tau'_{oi}/\mu_i). \quad (4)$$

Using equation (2) for θ, a solution for the minimum dip that can be reactivated is

$$\delta = \cos^{-1}\{(1 + \mu_f^2)^{-1/2} \times [\mu_f - (\mu_f/\mu_i)(C_{oi}H/2\tau_{oi}\cos^2\phi^e)]\}/2 + \tan^{-1}(\mu_f)/2 - \pi/4, \quad (5)$$

where a new constant is introduced:

$$C_{oi} \equiv 2[\mu_i + (1 + \mu_i^2)^{1/2}]\tau_{oi},$$

which is simply the compressive strength of the intact rock when μ_i is the internal (Coulomb) friction. The relation $\cos^{-1}x = \pi - \cos^{-1}(-x)$ can be used to write the expression for dip minima as

$$\delta = \pi/4 + \tan^{-1}(\mu_f)/2 - \cos^{-1} \times \{\mu_f(1 + \mu_f^2)^{-1/2}[(C_{oi}H/2\tau_{0i}\mu_i\cos^2\phi^e) - 1]\}/2. \quad (6)$$

The argument within the square brackets is a quantity that is greater than zero in all cases of weakening where dip-slip dominates oblique-slip (i.e. ϕ^e small). In the limit of small deviation in trend from that of newly breaking faults the first term in square brackets simplifies to

$$[1 + (1 + \mu_i^2)^{1/2}\mu_i^{-1}]H/(1 - \phi^{e^2}/2).$$

In the limit $\delta P' \to 0$, $\tau_{of} \to \tau_{oi}$ and $\mu_f \to \mu_i$; $H \to 1$. Then allowing $\phi^e \to 0°$ means that the term in square brackets becomes $\mu_i^{-1}(1 + \mu_i^2)^{1/2}$, reducing the argument of $\cos^{-1}$

in equation (6) to unity. In this limit the last term on the right-hand side of equation (6) vanishes, thus recovering the dip predicted by isotropic theory. It is important to recognize how the anisotropic term in equation (6) aids in reducing the allowed dip. Although previous studies (Bruhn *et al.* 1982, Sibson 1985) retained anisotropic effects, this last term on the right-hand side of equation (6) was not isolated. Equation (6) represents a more generalized lower bound than has been previously recognized.

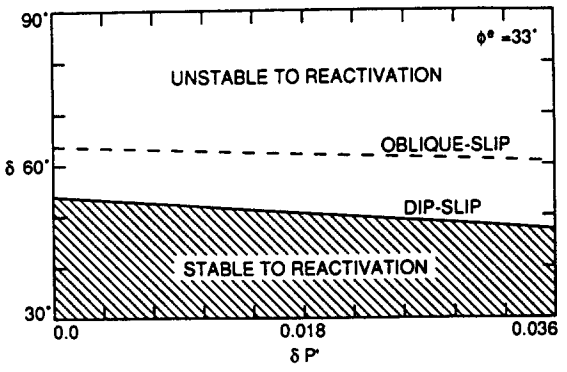

Fig. 3. Stability space examined for cases shown in Figs. 4–6. 'Stable' means no fault reactivation. The dashed line shows the position in δP – *dip* space where oblique-slip is marginally stable in an extensional stress field. This example is for the strike indicated and fault friction reduced by 20% from that of Byerlee's Law. Shown in Figs. 4–6 is the additional effect of strength contrast along a third axis and δP is scaled by δP_{max}, the maximum excess pore pressure allowable before tensile failure (see Fig. B1 in Appendix B).

ENHANCED PORE PRESSURE AND STRENGTH CONTRASTS

Simple plots of the stability space using the analytic results reveal how strength contrast and excess pore pressure shallow the allowed dip of normal faults. An example of the stability space is shown in Fig. 3 where a relatively oblique trend is assumed ($\phi^e = 33°$). Minimum allowed dip, δ, is plotted on the vertical axis and increasing excess pore pressure on the horizontal axis. The shaded region corresponds to shallow-dipping pre-existing structures that will *not* be reactivated before either breaking new 'Anderson' faults or sliding along optimally oriented prefractured rock characterized by Byerlee's Law.

For the oblique trend shown in Fig. 3 strike- (or 'oblique-') slip may be the preferred mode of failure on the pre-existing weakness. This potential dual behavior in the stability space is indicated by solid and dashed curves in Fig. 3. To obtain the minimum dip for the oblique-slip case a modified criterion for marginal stability was assumed (i.e. τ'_{ss} replaces τ'_{ds} in equation B7 of Appendix B). However, oblique-slip reactivation is not the primary focus of the discussion. In particular, we choose ϕ^e to be small such that dip-slip is always preferred and in Figs. 4–6 only normal faulting is considered. An additional bound (not shown in Figs. 3–6) limits the maximum steep dip that can be taken by a reactivated fault. In the Mohr diagrams shown in Figs. 2 and B1 this corresponds to the first intersection point of the failure envelope and circle.

Parameter study

In Figs. 4–6 the same stability space defined in Fig. 3 is visualized in three dimensions using frictional and cohesive strength contrast, μ_f/μ_i and τ_{of}/τ_{oi}, on an additional horizontal axis. The friction ratio, μ_f/μ_i, varies from $\frac{1}{4}$ to 1 and both cohesion ratio, τ_{of}/τ_{oi}, and enhanced pore pressure ratio, $\delta P/\delta P_{max}$, vary from 0 to 1 in Figs. 4–6. The surface shown in the space then corresponds to the minimum allowed dip as defined by equation (6).

Figure 4 shows the stability surfaces for three different crustal depths. The similarity of the surfaces among the three cases indicates that depth negligibly impacts the lower bound on reactivated dip. Note that reduction in cohesion (indicated by the surfaces on the right) reduces allowed dip by 6–15° while frictional reduction (left surfaces in Fig. 4) allows ≈40° lower dipping faults to be potentially reactivated. The relative uniformity in shape of the stability surfaces shown in Fig. 4 would not appear if not for the simple way in which the scaled excess pore pressure, $\delta P/\delta P_{max}$, reduces the allowed dip. The excess pore pressure is of maximum influence when strength contrasts are minimal (i.e. $\mu_f/\mu_i = 1$ and $\tau_o/\tau_{oi} = 1$, on the left and right in Fig. 4, respectively). In Fig. 4(a) the cohesional contrast assumed in constructing the surface to the left (μ_f/μ_i varying) is $\tau_{of}/\tau_{oi} = 1$. In this case the value of the dip predicted for intact rock obeying Byerlee's Law is recovered in the upper, far left-hand corner of the perspective plot (65.18° for $\mu_i = \mu_f = 0.85$).

Figure 5 shows two stability surfaces with a trade-off of slight strengthening due to small difference in trend (finite ϕ^e) vs strengthening due to cohesional annealing at the pre-existing fault surface (finite τ_{of}). The comparison of the two surfaces (a and b in Fig. 5) reveals the small influence that *slight* non-alignment in trend and cohesive annealing have in comparison to frictional contrast and pore pressure enhancement. Figures 5(a) & (b) were computed with identical intact rock parameters to facilitate a comparison of the depth-dependence.

Figure 6 shows the influence of 'dry' surrounding intact rock (a) and a fairly strict adherence to the popularly quoted forms of Byerlee's Law in two stress regimes (above and below a 200 MPa threshold) corresponding to two depths shown in frames (b) and (c). There is relatively little difference between 'wet' and 'dry' examples at 17 km depth (compare Fig. 6a with Fig. 4c). The ability of enhanced pore pressure to weaken low-angle faults does not appear to be a strong function of the fluid conditions of the intact rock; the overall effect is at most a few degrees.

The stability surfaces shown in Figs. 6(b) & (c) for 'wet' intact rock and cohesionless pre-existing fault rock show the most severe weakening in the limit of strong frictional contrast (i.e. low μ_f/μ_i). Like the surfaces shown in Fig. 4, the bound at the two depths is remarkably similar, despite the differences in intact strength.

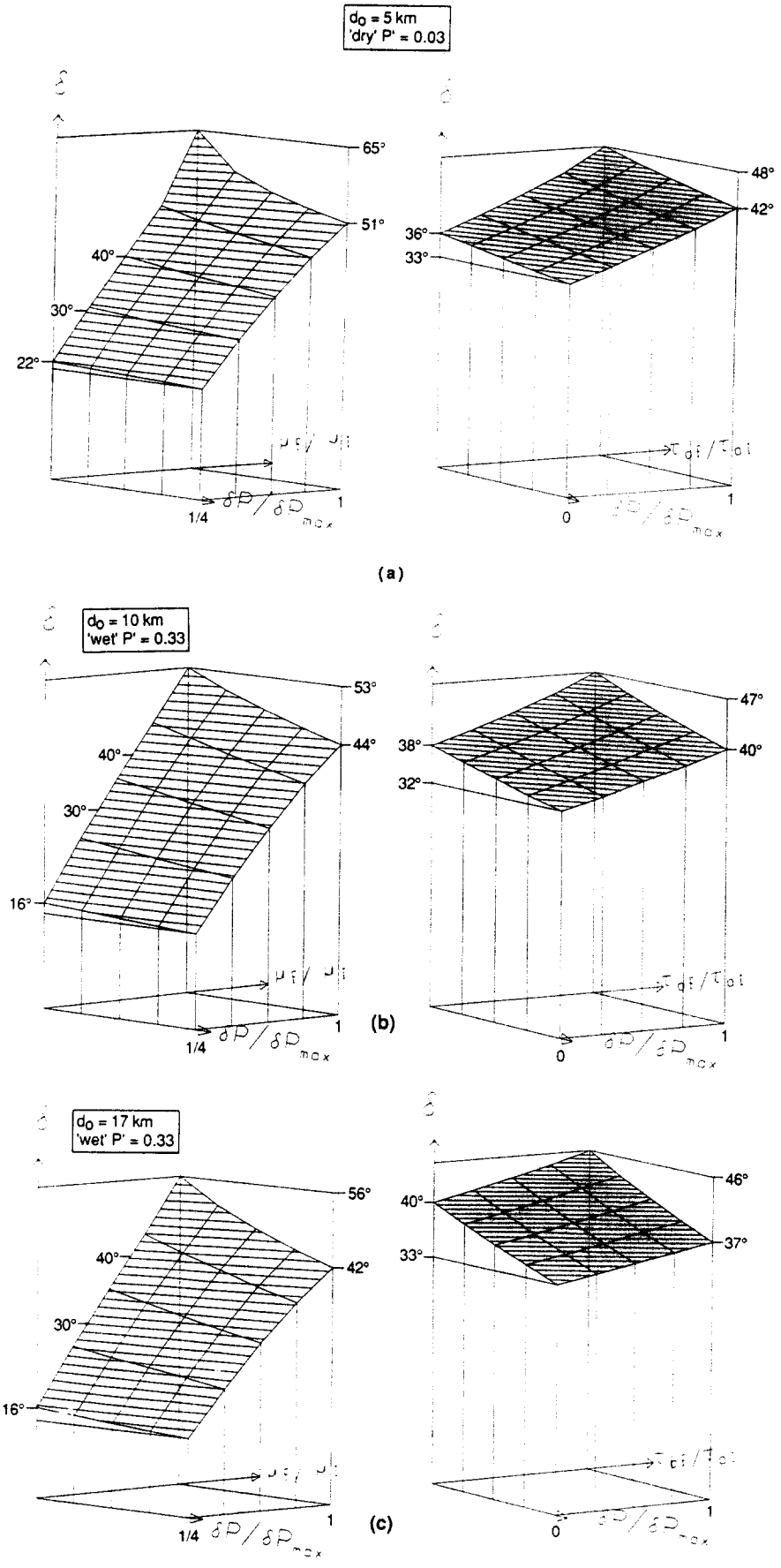

Fig. 4. Minimum allowed dip (δ) as a function of friction (left), cohesion reduction (right) and pore pressure enhancement at three depths. In all cases $\phi^e = 0°$, $\mu_i = 0.85$, $\tau_{oi} = 17.5$ MPa and $\mu_f/\mu_i = 0.75$ (for cases of cohesion variation), $\tau_{of}/\tau_{oi} = 0.5$ for cases of friction variation, except in (a) = 1.0. $\delta P/\delta P_{max}$ varies from 0 to 1. Each case on the left has μ_f/μ_i varying from $\frac{1}{4}$ to 1. Each case on the right has τ_{of}/τ_{oi} varying from 0 to 1. In (a)–(c) the values of σ_1 and S_r are: 1.32×10^2 MPa, (0.12); 2.65×10^2 MPa, (0.41); 4.50×10^2 MPa (0.44), respectively.

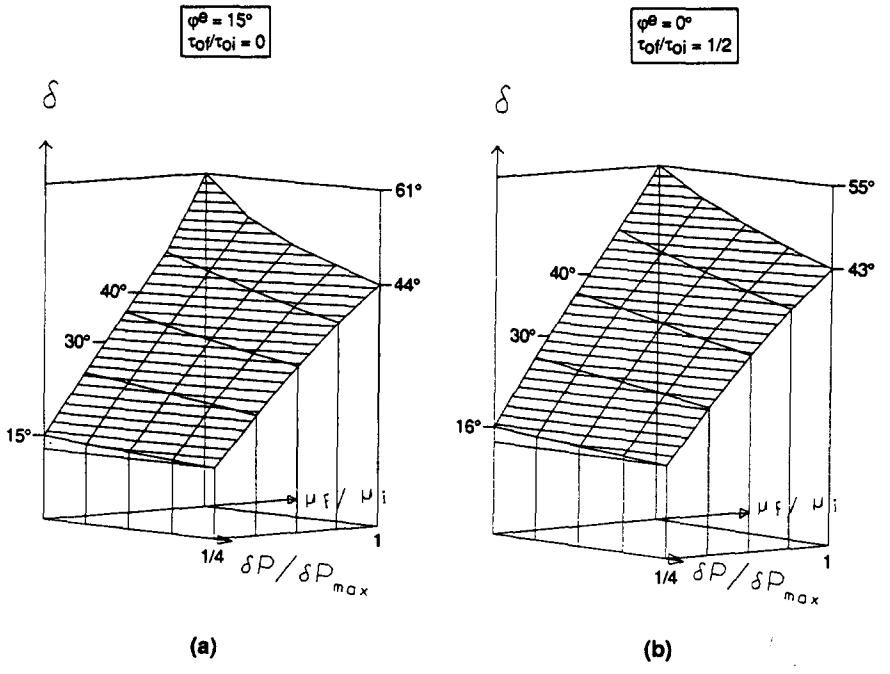

Fig. 5. Minimum allowed dip (δ) at d_o = 30 km. In both cases $\mu_i = 0.85$, $S_r = 0.43$, $\tau_{oi} = 35$ MPa, $P' = 0.33$ ('wet' intact rock). The numerical values for the varying ratios, μ_f/μ_i and $\delta P/\delta P_{max}$, are the same as in Fig. 4.

Lower bound

It can be shown that these last two cases (Figs. 6b & c) are exemplary of the lowest dip of a fault that is susceptible to reactivation, given the constraint that neither friction contrasts lower than $\frac{1}{4}$ or tensile failure are considered. Note that in equations (5) and/or (6) a diminished value for pore pressure factor, H, promotes dip shallowing. A minimum value for H in the case of 'dry' intact rock is, from equation (4),

$$\min\{H^{dry}\} \equiv \lim_{\delta P' \to S_r} H. \tag{7}$$

Using a 'dry' ($P' = 0$) value for S_r from equation (B2) of Appendix B, a cohesionless pre-existing fault ($\tau'_{of} = 0$ as in Figs. 6b & c) and the limit expressed in equation (7) then equation (6) reduces to:

$$\delta = \tan^{-1}(\mu_f), \tag{8}$$

representing the shallowest possible dip. It is important to note that equation (8) applies only in the limit $\delta P' \to S_r$, $P' \to 0$: two very severe restrictions. In equation (8) the values $\mu_f = 0.6/4$ and $\mu_f = 0.85/4$, yield 8° and 12° for δ. This 'shallowest possible' result is relatively uneffected by the level of intact fluid pressure, P', as evidenced by comparison of these values with the shallowest δ shown on the stability surfaces of Figs. 6(b) & (c). Equations (6) and (8) represent general and absolute bounds, respectively.

Summary of results and implications

Extremely shallow-dipping ($\leqslant 10°$) normal faulting caused by a nearly horizontal plane of anisotropy is possible without invoking either tensile failure or enhanced pore pressure on the fault relative to surrounding rock. However, anywhere in the brittle crust, including the base of the seismogenic zone, the static friction in a cohesionless pre-existing weakness must be $\leqslant 1/4$ of the nominal 'intact' value. The fact that a statistical ensemble of pre-existing faults is likely to exist that are of steeper dip and of equal (or greater) susceptibility to reactivation without such stringent requirements on frictional contrast casts doubt on brittle prefracture as a pervasive mechanism for the development of detachment surfaces in extensional tectonic terrains. Patterns of seismicity in active regions of continental extension support this conclusion (Jackson 1987a,b).

Numerous normal-slip seismic events occur with $30° \leqslant \delta \leqslant 40°$ in extensional tectonic environments (Arabasz & Julander 1986, Jackson 1987a,b). Equation (8) shows that when both cohesional and fluid pore pressure act with greatest dip reducing effect then fault reactivation with dip, $\delta = 30°$, corresponds to $\mu_f = 0.57$. A more realistic assessment of combined effects can be made by viewing the stability surfaces collectively in Figs. 4 and 6. A substantial fraction ($\geqslant \frac{1}{2}$) of the area of surfaces on the right in Figs. 4 and 6 (both have $\mu_f/\mu_i = \frac{3}{4}$) are below the value $\delta = 40°$.

Anisotropic MCA theory provides a way of placing bounds on the degree of misorientation that can be taken by a potential reactivating fault. In the limit $\delta P' \to 0$, $\mu_f \to \mu_i$, $\tau_{of} \to \tau_{oi}$, sliding on a pre-existing structure has no advantage over the breaking of new faults in intact rock. These limits are probably appropriate for the extremely low-angle normal faults that break across low-angle, pre-existing thrusts (e.g. Wernicke *et al.* 1985, 1986). Thus, while the hypothesis of brittle anisotropy reasonably accounts for seismic data, it falls short of fully explaining field observations of low-angle normal faults. A distinct lack of inherited weakness on pre-existing thrusts *and* rotation of the local principal

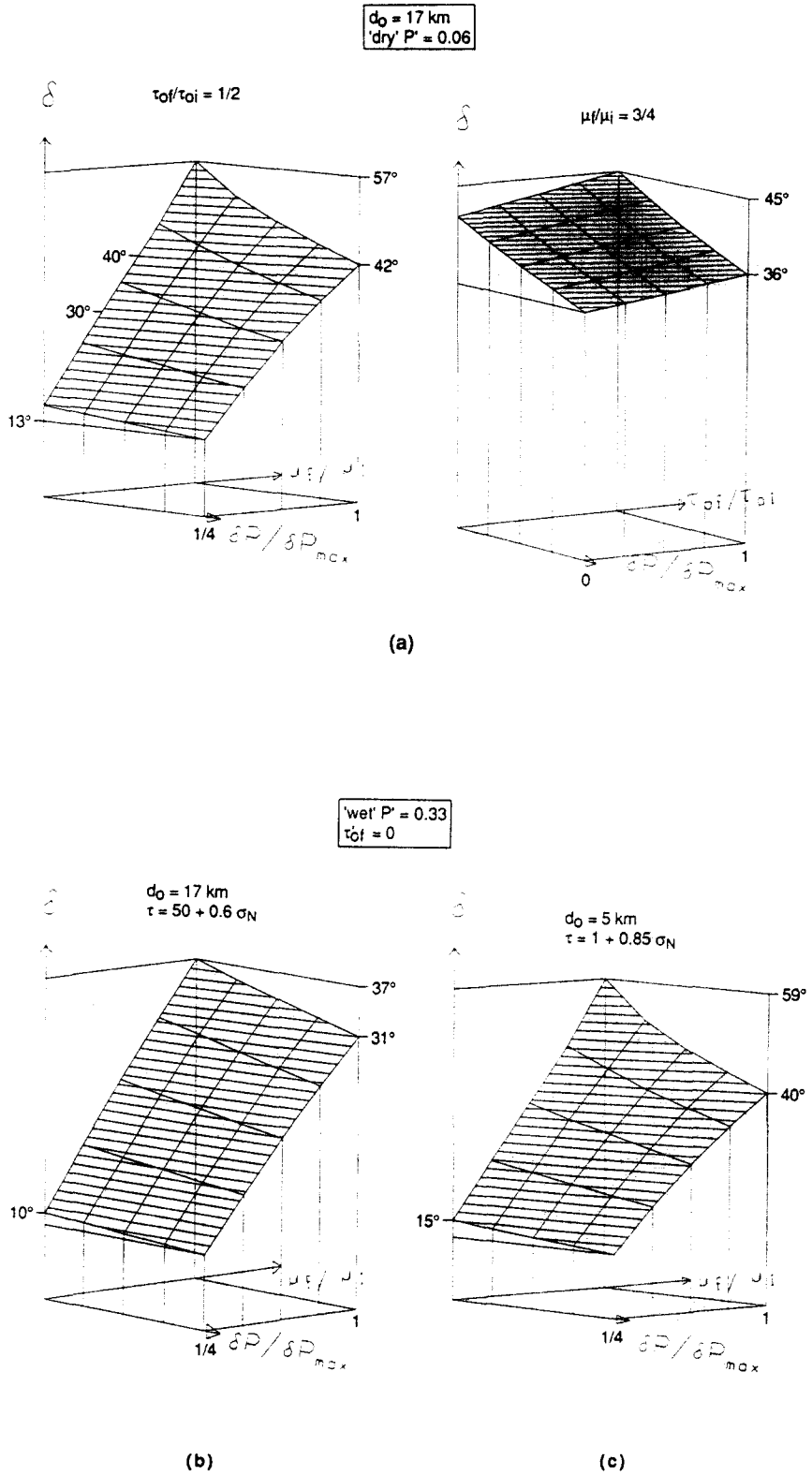

Fig. 6. Friction and cohesive influence with 'dry' intact rock (a) and friction influence alone at two depths (b & c) where differing lithostatic pressures require two forms of Byerlee's Law. (See two equation forms for τ the critical shear stress above b and c, respectively.) The small but finite cohesion in (c) has a negligible influence and is used to avoid singularity in equation (5). Stress ratios are S_r = 0.23, 0.42 and 0.47 for (a), (b) & (c), respectively. In (a) the friction coefficient and cohesion of intact rock are the same as those of Fig. 4. The numerical values for the varying ratios, μ_f/μ_i, τ_{of}/τ_{oi} and $\delta P/\delta P_{max}$, are the same as in Figs. 4 and 5.

stress system away from horizontal are required for MCA theory to predict extremely low-angle initial normal faults that crosscut low-angle abandoned thrusts.

CONCLUSIONS

The main result isolated by the analysis in this paper is that a single ratio:

$$H = (1 - P' - \delta P' + \tau'_{of}/\mu_f)/(1 - P' + \tau'_{oi}/\mu_i)$$

accounts for all the influence of pore pressure related effects and that a single factor:

$$(\mu_f/\mu_i)(1 + \mu_f^2)^{-1/2}\{\mu_i - C_{oi}H/[(2 - \phi^{e^2})\tau_{oi}]\}$$

accounts for all potential reduction in the allowed dip of normal faults due to brittle anisotropic effects. The ratio, H, demonstrates that pore pressure effects are maximum for $P' \to 0$ ('dry' intact rock), $\tau'_{of} \to 0$ (cohesionless pre-existing fault), large μ_f, τ'_{oi}, $\delta P'$ and small μ_i. Enhanced pore pressure (finite $\delta P'$) increases anisotropy most when all other factors are inhibitory. The factor shows that friction ratio, μ_f/μ_i, plays the largest role in exacerbating the chance that a low-angle pre-existing fault will be reactivated during extension. If the friction on the pre-existing fault is reduced by a factor of only $\frac{3}{4}$ with respect to wall rock, along with some combination of pore pressure enhancement and/or cohesion reduction, then shear failure of an abandoned thrust could account for normal faulting earthquakes on surfaces with dips of ≈30° as, for example, recently reported by Doser (1987) and Langer *et al.* (1987). The anisotropic form of Mohr–Coulomb–Anderson theory demonstrates that relatively moderate friction contrasts easily account for the shallowest normal-slip plane orientations reported by Arabasz & Julander (1986) and Jackson (1987a,b). Paucity of earthquakes on faults with dip shallower than 30° suggests that the shallowest reactivated fault surfaces are best characterized with static friction coefficients that are not less than about half those of nearby steeper faults.

Acknowledgements—Paul Tapponier is thanked for insightful discussions. We thank two anonymous reviewers for highly constructive criticism. This research was supported by NASA's Land Processes Office and was performed at Jet Propulsion Laboratory, California Institute of Technoloy.

REFERENCES

Allmendinger, R. W., Hauge, T. A., Hauser, E. C., Potter, C. J., Klemperer, S. L., Nelson, K. D., Knuepfer, P. & Oliver, J. 1987. Overview of the COCORP 40N transect, western United States: the fabric of an orogenic belt. *Bull. geol. Soc. Am.* **98**, 309–319.

Arabasz, W. J. & Julander, D. R. 1986. Geometry of seismically active faults and crustal deformation within the Basin and Range–Colorado Plateau transition in Utah. In: *Extensional Tectonics of the Southwestern United States: A Perspective on Processes and Kinematics* (edited by Mayer, L.). *Spec. Pap. geol. Soc. Am.* **208**, 43–74.

Barrientos, S. E., Stein, R. S. & Ward, S. N. 1987. Comparison of the 1959 Hebgen Lake, Montana and the Borah Peak, Idaho earthquakes from geodetic observations. *Bull. seism. Soc. Am.* **77**, 784–808.

Bergman, E. A. & Solomon, S. C. 1980. Oceanic intraplate earthquakes: implications for local and intraplate stress. *J. geophys. Res.* **85**, 5389–5410.

Brewer, J. A. & Smythe, D. K. 1984. MOIST and the continuity of crustal reflector geometry along the Caledonian–Appalachian orogen. *J. geol. Soc. Lond.* **141**, 105–120.

Bruhn, R. L., Yusas, M. R. & Huertas, F. 1982. Mechanics of low-angle normal faulting: an example from Roosevelt Hot Springs geothermal, area, Utah. *Tectonophysics* **86**, 343–361.

Burchfiel, B. C., Walker, J. D., Davis, G. & Wernicke, B. 1983. Kingston Range and related detachment faults—a major "breakaway" zone in the southern Great Basin. *Geol. Soc. Am. Abs. w. Prog.* **15**, 536.

Cloos, M. 1984. Landward-dipping reflectors in accretionary wedges: active dewatering conduits? *Geology* **12**, 519–522.

Coward, M. 1988. The Moine thrust and the Scottish Caledonides. In: *Geometries and Mechanisms of Thrusting, with Special Reference to the Appalachians* (edited by Mitra, G. & Wojtal, S.). *Spec. Pap. geol. Soc. Am.* **222**, 1–16.

Davis, D., Suppe, J. & Dahlen, F. A. 1983. Mechanics of fold-and-thrust belts and accretionary wedges. *J. geophys. Res.* **88**, 1153–1172.

Dixon, T. H., Stern, R. J. & Hussein, I. H. 1987. Control of Red Sea rift geometry by Precambrian structures. *Tectonics* **6**, 551–571.

Donath, F. P. & Cranwell, R. M. 1981. Probablistic treatment of faulting in geologic media. In: *Mechanical Behavior of Crustal Rocks* (edited by Carter, N. L., Friedman, M., Logan, J. M. & Stearns, D. W.). *Am. Geophys Un. Geophys Monogr.* **24**, 231–241.

Doser, D. I. 1987. The Ancash, Peru, earthquake of 1946 November 10: evidence for low-angle normal faulting in the high Andes of northern Peru. *Geophys. J. R. astr. Soc.* **91**, 57–71.

Enfield, M. A. & Coward, M. P. 1987. The structure of the West Orkney Basin, northern Scotland. *J. geol. Soc. Lond.* **144**, 871–884.

Engelder, T. & Marshak, S. 1988. Analysis of data from rock deformation-experiments. In: *Basic Methods of Structural Geology* (edited by Marshak, S. & Mitra, G.), Chap. 10. Prentice-Hall, Englewood Cliffs, New Jersey, 193–212.

Etheridge, M. A. 1986. On the reactivation of extensional fault systems. *Phil. Trans. R. Soc. Lond.* **A317**, 179–194.

Handin, J. 1969. On the Coulomb–Mohr failure criterion. *J. geophys. Res.* **74**, 5343–5348.

Heard, H. C. & Rubey, W. W. 1966. Tectonic implications of gypsum dehydration. *Bull. geol Soc. Am.* **77**, 741–760.

Hill, D. P. 1982. Contemporary block tectonics: California and Nevada. *J. geophys. Res.* **87**, 5433–5450.

Ivins, E. R. & Lyzenga, G. A. 1986. Stress patterns in an interplate shear zone: an effective anisotropic model and implications for the Transverse Ranges, California. *Phil. Trans. R. Soc. Lond.* **A318**, 285–347.

Jackson, J. A. 1987a. Active continental deformation and regional metamorphism. *Phil. Trans. R. Soc. Lond.* **A321**, 47–66.

Jackson, J. A. 1987b. Active normal faulting and crustal extension. In: *Continental Extensional Tectonics* (edited by Coward, M. P., Dewey, J. F. & Hancock, P. L.). *Spec. Publs geol. Soc. Lond.* **28**, 3–17.

Jaeger, J. C. 1960. Shear fracture of anisotropic rocks. *Geol. Mag.* **97**, 65–72.

Jaeger, J. C. 1969. *Elasticity, Fracture and Flow; With Engineering and Geological Applications*. Chapman & Hall, London, 268.

Langer, C. J., Bollinger, G. A. & Merghelani, H. M. 1987. Aftershocks of the 13 December 1982 North Yemen earthquake: conjugate normal faulting in an extensional setting. *Bull. seism. Soc. Am.* **77**, 2038–2055.

McKenzie, D. P. 1969. The relation between fault plane solutions for earthquakes and the directions of the principal stresses. *Bull. seism. Soc. Am.* **59**, 591–601.

Parry, W. T. & Bruhn, R. L. 1986. Pore fluid and seismogenic characteristics of fault rock at depth on the Wasatch fault, Utah. *J. geophys. Res.* **91**, 730–744.

Price, N. J. 1966. *Fault and Joint Development in Brittle and Semi-brittle Rock*. Pergamon Press, Oxford, 176.

Price, N. J. 1977. Aspects of gravity tectonics and the development of listric faults. *J. geol. Soc. Lond.* **133**, 311—327.

Price, R. A. 1967. The tectonic significance of mesoscopic subfabrics in the southern Rocky Mountains of Alberta and British Columbia. *Can. J. Earth Sci.* **4**, 39–70.

Raleigh, B. & Marone, C. 1986. Dilatancy of quartz gouge in pure shear. In: *Mineral and Rock Deformation: Laboratory Studies* (edited by Hobbs, B. E. & Heard, H. C.). *Am. Geophys. Un. Geophys. Monogr.* **36**, 1–10.

Ratcliffe, N. M., Burton, W. C., D'Angelo, R. M. & Costain, J. K.

1986. Low-angle extensional faulting, reactivated mylonites, and seismic reflection geometry of the Newark basin margin in eastern Pennsylvania. *Geology* **14**, 766–770.

Rundle, J. B. 1988. A physical model for earthquakes: 2. Application to southern California. *J. geophys. Res.* **93**, 6255–6274.

Secor, D. T. 1965. Role of fluid pressure in jointing. *Am. J. Sci.* **263**, 633–646.

Sibson, R. H. 1981. Fluid flow accompanying faulting: field evidence and models. In: *Earthquake Prediction: An International Review, Maurice Ewing Series* (edited by Simpson, D. W. & Richards, P. G.). *Am. Geophys. Un. Geophys. Monogr.* **4**, 593–603.

Sibson, R. H. 1985. A note on fault reactivation. *J. Struct. Geol.* **7**, 751–754.

Smith, R. B. & Bruhn, R. L. 1984. Interplate extensional tectonics of the eastern Basin-Range: inferences on structural style from seismic reflection data, regional tectonics, and thermal-mechanical models of brittle–ductile deformation. *J. geophys. Res.* **89**, 5733–5762.

Suppe, J. 1985. *Principles of Structural Geology*. Prentice-Hall, Englewood Cliffs, New Jersey, 537.

Sykes, L. R. 1978. Interplate seismicity, reactivation of pre-existing zones of weakness, alkaline magmatism, and other tectonism postdating continental fragmentation. *Rev. Geophys. & Space Phys.* **16**, 621–687.

Vrolijk, P. 1987. Tectonically driven fluid flow in the Kodiak accretionary complex, Alaska. *Geology* **15**, 466—469.

Webb, T. H. & Kanamori, H. 1985. Earthquake focal mechanisms in the eastern Transverse Ranges and San Emigdio Mountains, southern California and evidence for regional decollement. *Bull. seism. Soc. Am* **75**, 737–757.

Wernicke, B., Walker, J. D. & Beaufait, M. S. 1985. Structural discordance between Neogene detachments and frontal Sevier thrusts, central Mormon Mountains. *Tectonics* **4**, 213–246.

Wernicke, B., Hodges, K. V. & Walker, J. D. 1986. Geological setting of the Tucki Mountain area, Death Valley National Monument, California. In: *Mesozoic and Cenozoic Structural Evolution of Selected Areas, East-Central California Guidebook*. Geological Society of America, Boulder, Colorado.

Wojtal, S. & Mitra, G. 1986. Strain hardening and strain softening in fault zones from foreland thrusts. *Bull. geol. Soc. Am.* **97**, 674–687.

Zoback, M. L. & Zoback, M. 1980. Faulting patterns in north-central Nevada and strength of the crust. *J. geophys. Res.* **85**, 275–284.

APPENDIX A: GEOMETRY

The geometrical aspects of the connection between fault plane orientation (with respect to driving-tectonic stress) and critical stress criteria for reactivation are derived here and the basic governing formulas stated. Only the simplest assumptions regarding the stress caused by regional extension will be considered.

The fault is considered to coincide with the x'–y' plane of the co-ordinate system x',y',z'. The crust of non-variable thickness lays flat in the x–y plane of co-ordinate system x,y,z (cf. Figs. 1 and A1). The convention that the tectonic stress acts in the x direction is employed. The angle ϕ^e (strike) is measured counterclockwise from the y axis as shown in Fig. 1. The x,y,z frame is the principal stress co-ordinate frame, with the z-axis corresponding to the maximum principal stress, $\sigma_1 = \rho g d_o = \sigma_{zz}$.

In an extending crust the usual assumption is that the intermediate principal stress is lithostatic (i.e. equal to the overburden, σ_1). This condition can never be assumed to be exact (e.g. Zoback & Zoback 1980). The tectonic stress could be superimposed on a Poisson stress state (Jaeger 1969, p. 171). However, it can be shown that this latter stress state yields only negligible differences when considering the reactivation of shallow-dipping normal faults. Consequently, the analysis given below and in Appendix B assumes lithostatic σ_1. The lithostatic stress with no tectonic stress is then; $\sigma_{xx} = \sigma_{yy} = \rho g d_o$ (Heim's Rule). Superposition of a reference normal tectonic stress, c_x, then produces a principal stress set:

$$\sigma_{xx} = c_x + \rho g d_o \tag{A1a}$$

$$\sigma_{yy} = -c_x + \sigma_{xx} \tag{A1b}$$

and for ambient extension, $c_x < 0$. In (A1a) and (A1b) $\mathbf{g}$ is gravitational acceleration and d_o is the depth of the seismogenic crustal portion where reactivation may occur. In the analysis c_x enters through the ratio $S_r = \sigma_{xx}/\sigma_{zz}$:

$$S_r = 1 - |c_x|/\rho g d_o. \tag{A2}$$

It is important to note that S_r is determined by the MCA stability criterion applied to the intact rock. Further clarification of this point is given in Appendix B.

In order to fully state the stability criterion for a pre-existing fault plane in x'–y' (Figs. 1 and A1) the principal stress system, $\sigma_{xx}, \sigma_{yy}, \sigma_{zz}$, must be resolved there. In the primed frame shown in Fig. A1 the shear

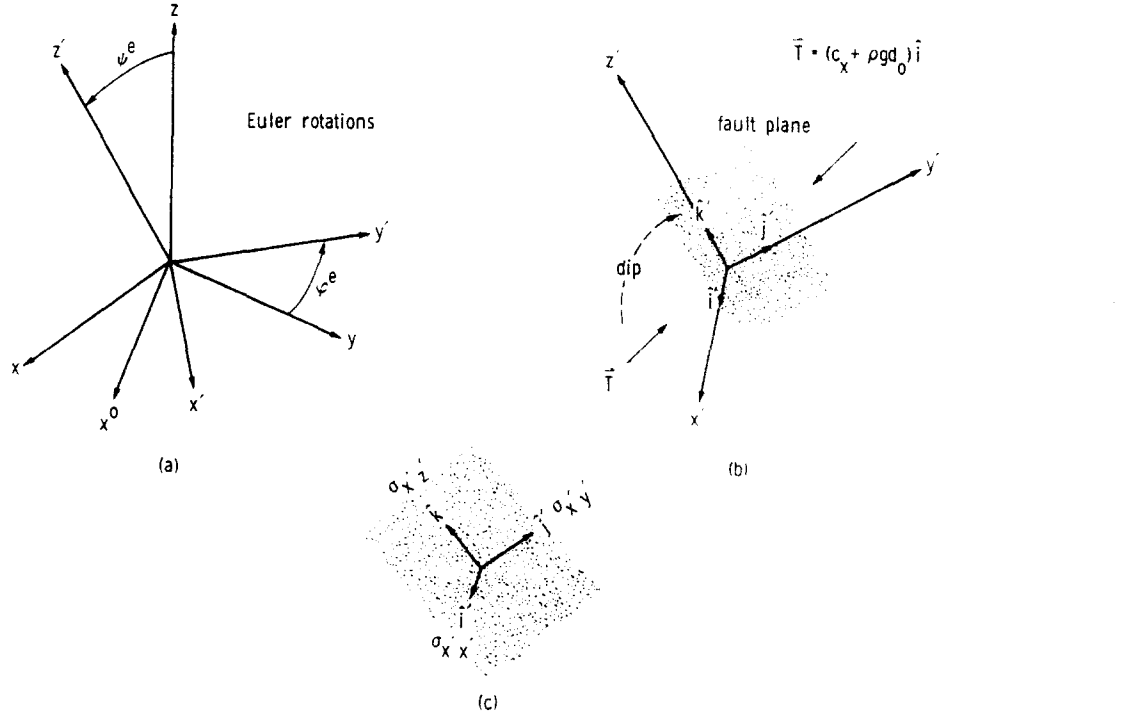

Fig. A1. Pre-existing fault plane (b & c) and total extensional tectonic driving force in the x-direction (c). Transformations from principal stress axes to primed frame are shown in frame (a). Resolved stress components shown in (c) are discussed in Appendix A.

inducing dip-slip is $\sigma_{x'z'}$ while that inducing oblique-slip is $\sigma_{x'x'}$. There exists an Euler rotation, ψ^e, that, together with rotation through ϕ^e, defines the rotation tensor **A** relating primed and unprimed tensor quantities. The second-rank stress tensor of the principal stress system, $\boldsymbol{\sigma}'$, is related to the stress tensor in the fault plane co-ordinates, $\boldsymbol{\sigma}'$, by the 4th-rank rotation tensor **AA**, where **A** is formed from the components of the rotation tensor. Specifically,

$$\boldsymbol{\sigma}' = \mathbf{AA}\boldsymbol{\sigma}, \tag{A3}$$

consistent with Zoback & Zoback (1980, equation 3). The detailed expressions for **A** have been given by Ivins & Lyzenga (1986, equation 4). Identifying the Euler rotation ψ^e as $\pi/2 - dip$, two relevant shear stresses, $\sigma_{x'z'}$ and $\sigma_{x'y'}$, and one normal stress $\sigma_{x'x'}$, resolved at the fault surface can be determined by using a series of unit vector dyadic operations on (A3). The results are

$$\tau_{ds} = \sigma_{x'z'} = \sin(2\,dip)(\sigma_{zz} - \sigma_{xx}\cos^2\phi^e - \sigma_{yy}\sin^2\phi^e)/2 \tag{A4a}$$

$$\tau_{ss} = \sigma_{x'y'} = \sin(dip)\sin 2\phi^e(\sigma_{xx} - \sigma_{yy})/2 \tag{A4b}$$

$$\sigma_N = \sigma_{x'x'} = \sin^2(dip)[\sigma_{xx}\cos^2\phi^e + \sigma_{yy}\sin^2\phi^e + \sigma_{zz}\cot^2(dip)], \tag{A4c}$$

where subscripts 'ds', 'ss', 'N', refer to dip-slip, oblique-slip and normal stress components, respectively. A normal faulting regime occurs when the maximum principal stress is vertical and the minimum is coincident with the direction of extension. Hence, setting $\sigma_1 = \sigma_{zz}$, $\sigma_2 = \sigma_{yy}$, $\sigma_3 = \sigma_{xx}$ and using equations (A2) and (A3),

$$\sigma_1 = \rho g d_o \tag{A5a}$$

$$\sigma_2 = \rho g d_o \tag{A5b}$$

$$\sigma_3 = S_r \rho g d_o. \tag{A5c}$$

The ratio of the resolved shear stresses inducing oblique-slip to those for dip-slip can be written by using equations (A5) and (A4):

$$|\tau_{ss}/\tau_{ds}| = \tan\phi^e \sec(dip). \tag{A6}$$

Generalizing the right-hand side of equation (A6) to include the effect of intermediate stress, σ_2, that deviates from σ_1 by an amount $+(\sigma_3 - \sigma_1)R$, simply involves a multiplicative factor, $[(1 - R)/(1 + R\tan^2\phi^e)]$. Usually R is expressed as the ratio $(\sigma_2 - \sigma_1)/(\sigma_3 - \sigma_1)$.

APPENDIX B: MARGINAL STABILITY STATE

Stability of the crust to the reactivation of pre-existing weaknesses in the presence of waxing extensional forces occurs when relatively unfaulted, 'intack', rock suffers extensive breakage, thus, reducing, or equilibrating, regional stress. Subsequent finite deformational extension then ensues by utilizing newly broken faults. Instability, on the other hand, is defined when the pre-existing fault renews its activity and becomes a spatio-temporal impediment to breakage of new faults. It is important to keep in mind that stability can be defined only when a yield stress is involved. If fault movement is controlled by ductile processes, such as those caused by grain size reduction and pressure solution (Wojtal & Mitra 1986), then viscous deformation occurs at any applied stress level and the question of stability is inappropriate.

The stability of a pre-existing brittle fault can be established by first examining the Mohr circle of intact rock. The frictional constitutive law for intact rock is

$$\tau = \tau_{oi} + \mu_i(\sigma_N - P), \tag{B1}$$

where τ_{oi} and μ_i are the cohesion and friction parameters of the intact rock, respectively, as described in Fig. 1. The fluid pore pressure of intact rock is P. Any tectonic stress, c_x, leads to a stress state characterized by an infinite family of circles, each intersecting the tangent line (B1) in τ vs $\sigma_N - P$ space (see Fig. 2, for example). The radius, τ_m, of each circle is $3/2\sqrt{2}$ of the octahedral shear stress. The center of each circle is determined by the mean stress, $\sigma_m \equiv (\sigma_1 + \sigma_3)/2$. A single circle of the infinite family is then specified when the analysis is applied to a unique depth, d_o; a position at which the effective overburden, $\rho g d_o - P$ is the maximum effective principal stress. The equation (B1) and the Mohr circle, determined by the condition of tangency and effective overburden, completely specify the reference stress state of the stability problem. As stated above, the value of the tectonic stress, c_x is then superfluous to the analysis that follows. In this regard, it should be noted that the tangency condition is

$$S_r = \{2[\mu_i(P' - 1/2) - \tau'_{oi}] + (1 + \mu_i^2)^{1/2}\} \div [\mu_i + (1 + \mu_i^2)^{1/2}] \tag{B2}$$

and, consequently the value of the tectonic stress may be recovered from equations (A2) and (B2). In equation (B2) $P' \equiv P/\sigma_1$ and $\tau'_{oi} \equiv \tau_{oi}/\sigma_1$. It may be noted that equation (B2) can be recovered from the basic equation used by Bruhn *et al.* (1982) and by Sibson (1985) (see equations 1 and 3, therein, respectively) through selection of the optimum angle for faulting $\pi/4 + \tan^{-1}(\mu)/2$.

When the pre-existing fault has an extra amount of pore pressure, $\delta P'$, above that of the nominal intact rock, and a differing, lower, cohesion, τ'_{of}, and friction, μ_f, then the critical failure envelope may be written as:

$$\tau'_{fc} = \tau'_{of} + \mu_f(\sigma'_N - P' - \delta P'). \tag{B3}$$

Since the stress state is determined by intact rock strength (equation B2) and the depth, d_o, then the dip-slip component of stress (equation A4a) can be written as:

$$\tau'_{ds} = \sin(2\,dip)(1 - S_r\cos^2\phi^e - \sin^2\phi^e)/2. \tag{B4}$$

If

$$\tau'_{ds} > \tau'_{fc}, \tag{B5}$$

reactivation of pre-existing faults supersedes breakage of new faults. When inequality (B5) holds then the plane of anisotropy is *unstable* to

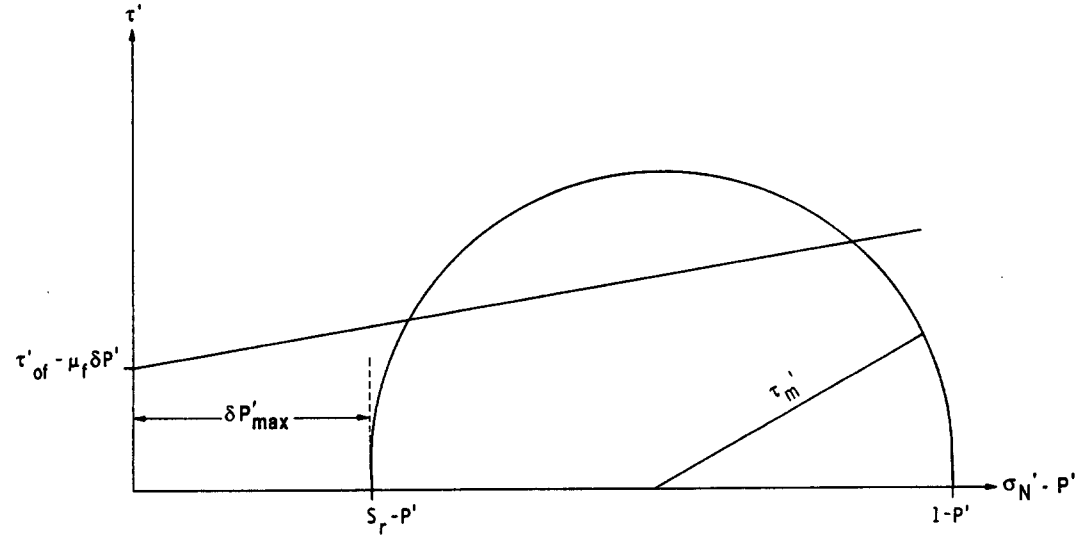

Fig. B1. Dimensionless Mohr circle with $\phi^e = 0°$ and pre-existing fault failure envelope. (See equations B3 and B6.)

fracture. In the case $\varphi^c = 0°$ equation (B4) can be equated with a dimensionless critical stress (equation B1 divided by σ_1) to yield

$$\tau'_m \sin(2dip) = \tau'_{oi} + \mu_i(\sigma'_N - P'). \quad \text{(B6)}$$

where the dimensionless mean shear stress is, $\tau'_m \equiv (1 - S_r)/2$. Equation (B6) is recognized as the equation for a circle of radius τ'_m in polar co-ordinates with the counterclockwise directed angle $2dip$ (see Figs. 2 and B1). In Fig. B1 this circle is shown with the intersecting failure envelope for the pre-existing fault. Also shown in Fig. B1 is the maximum extra pore pressure, δP_{max}, on the pre-existing fault possible without tensile failure occurring. In the dimensionless Mohr diagram of Fig. B1 *all* faults with dips represented by the arc subtending the two intersection points of the line with the circle are *unstable* to reactivation (Handin 1969, Donath & Cranwell 1981). The *marginal stability state* is defined when a single shallow fault of given dip, δ, is as *equally susceptible* to reactivation as is intact rock to breaking with new normal faults of dip, $\Delta = \pi/4 + \tan^{-1}(\mu_i)/2$. In the marginal state

$$\tau'_{ds} = \tau'_{ic}. \quad \text{(B7)}$$